CSIRO PUBLISHING

www.publish.csiro.au/journals/ijwf *International Journal of Wildland Fire*, 2004, **13**, 275–285

A dynamic algorithm for wildfire mapping with NOAA/AVHRR data

R. Pu[A,B], *P. Gong*[A,B,D], *Z. Li*[C] *and J. Scarborough*[B]

[A]State Key Lab of Remote Sensing Science, IRSA, Box 9718, Beijing 100101, China.
[B]Center for Assessment and Monitoring of Forest and Environmental Resources, 151 Hilgard Hall, University of California, Berkeley, CA 94720-3110, USA. Telephone: +1 510 642 1351; fax: +1 510 643 5098; email: rpu@nature.berkeley.edu; gong@nature.berkeley.edu; jscar@gisc.berkeley.edu
[C]Department of Meteorology and Earth System Science Interdisciplinary Center, University of Maryland, College Park, MD 20742-2425, USA. Telephone: +1 301 405 6699; fax: +1 301 405 8468; email: zli@atmos.umd.edu
[D]Corresponding author.

Abstract. A wildfire-mapping algorithm is proposed based on fire dynamics, called the dynamic algorithm. It is applied to daily NOAA/AVHRR/HRPT data for wildland areas (scrub, chaparral, grassland, marsh, riparian forest, woodland, rangeland and forests) in California for September and October 1999. Daily AVHRR images acquired from two successive days are compared for active fire detection and burn scar mapping. The algorithm consists of four stages: data preparation; hotspot detection; burn scar mapping; and final confirmation of potential burn scar pixels. Preliminary comparisons between the result mapped by the dynamic algorithm and the fire polygons collected by the California Department of Forestry and Fire Protection through ground survey indicate that the algorithm can track burn scars at different developmental stages at a daily level. The comparisons between wildfire mapping results produced by a modified version of an existing algorithm and the dynamic algorithm also indicate this point. This is the major contribution of this algorithm to wildfire detection methods. The dynamic algorithm requires highly precise registration between consecutive images.

Introduction

Quantitative information about the spatio-temporal distribution of wildfires is indispensable to fire ecology, wildlife management and atmospheric chemistry and forestry (Levine 1991). Wildfire is an important factor in ecosystem management, land cover change and wildlife habitat studies (Levine 1991; Pozo *et al*. 1997; Rauste *et al*. 1997; Li *et al*. 2000*a*). Vegetation fires emit substantial amounts of trace gases (e.g. CO_2, CO, CH_4, NO_X) and particulates into the atmosphere (Andreae *et al*. 1996). They affect human health and the Earth's radiation budget (Franca *et al*. 1995). Remote sensing of fires has been achieved using a variety of space-borne systems/sensors. In the last decade, the most widely used sensor for long-term and large-scale fire monitoring has been the Advanced Very High Resolution Radiometer (AVHRR) on board the National Oceanic and Atmospheric Administration's (NOAA) polar orbiting satellites (Flannigan and Vonder Haar 1986; Kaufman *et al*. 1990; Kennedy *et al*. 1994; Justice *et al*. 1996; Li *et al*. 1997; Pereira 1999; Stroppiana *et al*. 2000).

AVHRR (onboard the NOAA-14 satellite) imagery was chosen for its 1.1 km medium resolution, large geographical coverage with a swath width exceeding 2500 km, and excellent daily sampling frequency (Cahoon *et al*. 1992). It provides information over a large geographical area with potentially more cloud-free scenes for fire monitoring than other sensors' images, such as Landsat TM images. In addition, the spectral bandwidths of AVHRR data offer considerable benefits to fire monitoring (Harris 1996; Li and Giglio 1999). Channels 1 and 2 (visible and near-infrared channels) provide data capable of detecting, monitoring and measuring smoke emissions (Kaufman *et al*. 1990; Khazenie and Richardson 1993). Channel 3 (mid-infrared) is extremely sensitive to hot spots at the subpixel level. Although it has a lower temperature saturation point, ~321 K, it is the most important channel for fire detection (Muirhead and Cracknell 1985; Setzer and Pereira 1991; Franca *et al*. 1995; Pozo *et al*. 1997; Rauste *et al*. 1997). Channels 4 and 5 (thermal channels) are far less sensitive to subpixel hotspots, but they are often helpful to fire detection when combined with the other channels (Flasse and Ceccato 1996; Justice *et al*. 1996). In addition, the AVHRR onboard post-NOAA-14 satellite includes a 1.65 μm short wave infrared (SWIR) channel. The SWIR channel has proven to be highly effective

 10.1071/WF03054 1049-8001/04/030275

for discriminating burned boreal forest (e.g. Fraser and Li 2002).

Existing methods of wildfire detection using NOAA/AVHRR data can be divided into two broad categories (Giglio *et al*. 1999; Li *et al*. 2000*a*): (1) fixed threshold algorithms including single channel threshold using channel 3 and multi-channel thresholds using two or more AVHRR channels; and (2) adaptive threshold contextual algorithms. Fixed threshold algorithms apply empirically defined thresholds to discriminate pixels containing fires from those of non-burning surroundings and clouds (Boles and Verbyla 2000). With this category of algorithm, varying degrees of success in fire detection have been reported (Flannigan and Vonder Haar 1986; Kaufman *et al*. 1990; Kennedy *et al*. 1994; Li *et al*. 1997, 2000*a*; Pozo *et al*. 1997; Rauste *et al*. 1997; Arino and Mellinotte 1998). The advantage of these types of algorithms is their computational simplicity. Their limitation is that fixed thresholds are applicable only at local to regional scales during a short fire season.

Contextual algorithms use adaptive thresholds for fire detection. The flexible threshold algorithms identify a fire pixel based on the level of contrast between the potential fire pixel and its 'background' pixels (the definition of background varies according to kernel size) (Boles and Verbyla 2000). Contextual algorithms are believed to be flexible and effective in a range of different environmental conditions (Flasse and Ceccato 1996). Therefore, a contextual algorithm adapted from Flasse and Ceccato (1996) is being used by the International Geosphere–Biosphere Programme, Data and Information Systems (IGBP-DIS) fire product (Justice and Dowty 1994; Malingreau and Justice 1997; Dwyer *et al*. 1998; Stroppiana *et al*. 2000). In principle, contextual methods are more versatile for application to a wide range of conditions than fixed threshold approaches. However, the initial fire detection involves fixed thresholds. When they are set too high, there is a risk of omitting candidate fire pixels during the contextual processing stages of fire confirmation (Li and Giglio 1999).

Active fire detection can identify only a portion of the entire burn scars due to clouds and infrequent satellite overpass (Li *et al*. 2000*b*). Burn scar mapping should be considered as another aspect of wildfire mapping in order to obtain a precise burn scar map. According to Arino *et al*. (1999), extraction of burn scars from AVHRR data can be performed with three different approaches: (1) application of multiple tests to spectral values or derived indices (Pereira 1999) on a single date basis; (2) temporal analysis of derived indices based on pre- and post-fire images; and (3) classical image segmentation techniques (e.g. use of unsupervised and supervised classifiers) with single date or multi-date imagery. Furthermore, a new type of burn-scar mapping algorithm has been proposed that combines an active-fire detection algorithm with NDVI and/or other vegetation indices differencing. For example, one technique, known as HANDS (Hotspot and NDVI Differencing Synergy), combines the strengths of its two constituent techniques while avoiding their limitations (Fraser *et al*. 2000). Another example is a methodology based on a combination of AVHRR active-fire detections and a time series of NDVI where NDVI was computed with an AVHRR middle-infrared channel instead of a visible channel to reduce the impact of smoke aerosols (Roy *et al*. 1999). In addition, Roy *et al*. (2002) developed a new method applicable to burned area mapping using multi-temporal moderate spatial resolution data (MODIS: the MODerate resolution Imaging Spectroradiometer, onboard EOS series satellites). They compared the MODIS observations through time with the bi-directional reflectance model-based expectation values to detect burned area.

Recently, MODIS imagery has become another source of data of appropriate spatial and temporal resolution to be used for global studies of biomass burning (Kaufman *et al*. 1998). Fundamentally, these active-fire detection and burn scar mapping algorithms, reviewed briefly above, can be modified and applied to MODIS data.

Existing algorithms for active-fire detection and burn scars mapping lack daily fire evolution tracking capability from AVHRR data, especially for burn scars mapping, although some algorithms can compute such evolution tracking within a relatively wide time period (e.g. within an NOAA satellite repeat cycle (Roy *et al*. 1999)) or can detect approximately daily burning using multi-temporal MODIS data (Roy *et al*. 2002). In this paper, we propose a new algorithm based on fire dynamics at a daily scale to obtain daily hotspots and burn scars. It was applied to California using AVHRR data acquired over two months, September and October 1999. The results generated by the new algorithm are presented and analysed.

Data source and preprocessing

AVHRR data

Daytime AVHRR-HRPT (High Resolution Picture Transmission format) images (1.1 km resolution at nadir) were acquired daily by NOAA-14. The AVHRR-HRPT data were downloaded directly from the NOAA Satellite Active Archive Data Center (http://www.saa.noaa.gov). The local overpass time of NOAA-14 over California during the two months varied from 14:00 to 15:30. The dataset covers the entire state of California. Due to excessive cloudiness and a data acquisition problem, 13 September and 4, 11, 26 and 27 October were missed. Consequently, only 56 daily images were available for analysis. NDVI was calculated from channels 1 and 2 through (Ch2−Ch1)/(Ch2+Ch1). An incomplete dataset of fire polygons collected through ground survey by the California Department of Forestry and Fire Protection (CDF) and wildfire mapping results produced by other wildfire detection algorithms with the same dataset as those used for testing the

dynamic algorithm were used to validate results produced in this experiment.

Data preprocessing

The PACE AVHRR Orbital Navigation Package (PCI geomatics company, Canada, 1997) was used to preprocess AVHRR data using calibration/orbit information and extracted ground control points from the AVHRR data file. High precision geometric correction and registration were accomplished by running PCI-OrthoEngine (PCI Geomatics company, Canada, 1999). Because the scan angle of the AVHRR sensor is quite large (~110.8°), the solar zenith angle can vary significantly along a scanline, causing different parts of an AVHRR image to receive varying amounts of solar radiation. The radiance imbalance among pixels can be reduced by a radiometric (solar zenith angle) correction (Di and Rundquist 1994). Percentage reflectance from the top of the atmosphere (TOA) for channels 1 and 2 and surface brightness temperature in Kelvin for thermal channels were obtained. With 6–10 ground control points (GCPs) collected manually from each of the images over the two-month period, we achieved a georeferencing accuracy of better than 1 km for most images in the time series.

Algorithm

The flowchart of the dynamic algorithm proposed in this study is shown in Fig. 1. It is divided into four components corresponding to preparation, hotspot detection, burn scar detection and final confirmation.

Preparation (Fig. 1a)

To map wildfires, the dynamic algorithm needs images from two consecutive days, the present day (D2) and the day before (D1). The algorithm requires all channels of raw data for D2 but only the NDVI (denoted by $NDVI_{D1}$) and cumulative hotspot and burn scar results for D1. In order to eliminate pixels on the D2 image contaminated by clouds, cloudy pixels are identified through two tests: brightness temperature channel 3 < 260 K and reflectance channel 1 > 80% (brightness temperature channels 3, 4 and 5, hereafter denoted as T3, T4 and T5, and reflectance channels 1 and 2, hereafter, denoted as R1 and R2). If for a pixel on the D2 image T3 < 260 K and R1 > 80%, it is considered a cloudy pixel (Lee and Tag 1990; Malingreau and Justice 1997); this is because for clouds, brightness temperature in MIR is low and reflectance in the visible region is high. The NDVI and burn status of cloudy pixels from D2 are replaced with those of D1 in the later analysis. The burn status of a pixel is divided into three classes: hotspot, burn scar and normal (unchanged). To reduce the different solar elevation effect on NDVI, $NDVI_{D2}$ is normalised to $NDVI_{D1}$. This is achieved by balancing the NDVI means of D1 and D2. NDVI difference (NDVIdiff) between D1 and D2 is calculated by subtracting $NDVI_{D1}$ from normalised $NDVI_{D2}$. Finally, the mean and standard deviation (s.d.) of NDVI decrease between D1 and D2 are calculated over the regions of the different land cover types. It is worth noting here that, since the NDVI values of D1 and D2 are calculated with the TOA reflectance of channels 1 and 2, if it happens that the phenomenon of sudden and dramatic impact of smoke aerosols on TOA reflectance occurs when the satellite overpasses, the NDVI values may not be reliable. However, due to difficulties in reliable atmospheric correction of smoke aerosols, we still use the NDVI calculated with the TOA reflectance and try to weaken the resulting impact of the smoke aerosols and the variation of other atmospheric components on NDVI by normalising $NDVI_{D2}$ to $NDVI_{D1}$.

Hotspot detection (Fig. 1b)

As in most previous work (Kennedy *et al*. 1994; Franca *et al*. 1995; Justice *et al*. 1996; Arino and Mellinotte 1998; Li and Giglio 1999; Li *et al*. 2000*a*), tests based on brightness temperature (T3 ≥ 315 K) and NDVI difference (NDVIdiff < (mean + 1.0 * s.d.)) for any pixel are first assessed to determine if it is a potential fire pixel. The threshold for T3 was selected based on the assumption that the radiation measured by channel 3 corresponded to peak radiation from objects around 800 K. This is close to the burning temperature of biomass (Kennedy *et al*. 1994), although most wildfires will range from 500 K to 1000 K (Li *et al*. 2000*a*). The threshold for NDVIdiff was set by trial-and-error with data from known burn scars (CDF fire polygons). An NDVI difference lower than the threshold is considered indicative of burning biomass (note that this condition is not available in existing active-fire detection algorithms). Otherwise, the vegetation falls in the non-burnt category. Therefore, an NDVI difference threshold can filter out a certain percentage of the false fires that pass the condition T3 ≥ 315 K.

The remaining five tests at this stage are for removing false fires. The thresholds of the five tests are similar to those used elsewhere (e.g. Li *et al*. 2000*a*). The threshold for (T3–T4) eliminates false fires caused by warm background. In southern California, bare soils can be a warm background that during the daytime saturates channel 3. In the event of biomass burning, channel 3 receives much more radiant energy than channel 4. Therefore, T3–T4 is high (Kennedy *et al*. 1994; Li *et al*. 2000*a*). Test T4 ≥ 260 K eliminates pixels with highly reflective clouds. Test (T4–T5) ≥ 4 K and (T3–T4) ≤ 19 K, as in Li *et al*. (2000*a*), is for eliminating false fire pixels caused by thin cirrus clouds and for further removing the false fires, caused by warm background, that passed the previous tests. The remaining two tests eliminate false fires caused by highly reflecting clouds, bright surfaces ((R1+R2) ≥ 75% and R2 ≥ 30%) and sun glint pixels (|R1−R2| ≤ 1%).

Burn scar detection (Fig. 1c)

At the second stage of analysis—burn scar detection—we first check if T3 < 315 K for a given pixel. If that is true

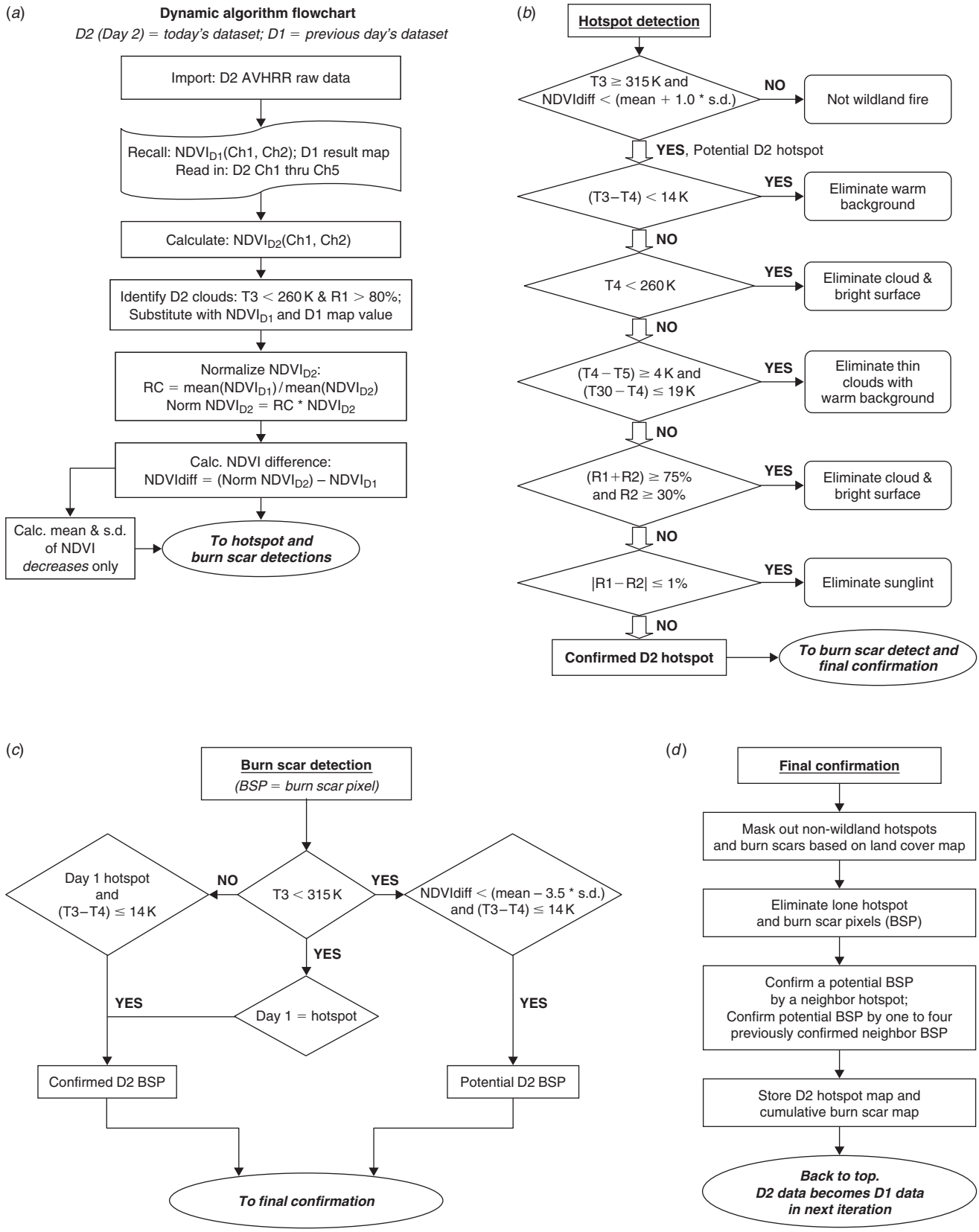

Fig. 1. A flowchart of the dynamic algorithm. (*a*) Preparation stage. (*b*) Hotspot detection stage. (*c*) Burn scar detection stage. (*d*) Final confirmation stage.

and the pixel was a hotspot pixel on D1, then it automatically becomes a confirmed burn scar pixel (BSP) on D2. If T3 < 315 K but it was not a hotspot on D1, then the pixel may satisfy NDVIdiff < (mean − 3.5 * s.d.) and (T3–T4) ≤ 14 K, in which case it is a potential BSP. Otherwise it is considered a normal pixel (unburned pixel). A coefficient of 3.5 was determined based on the criterion of minimum residual error through analysis of difference between the actual burn scars selected from CDF fire polygons and the corresponding mapped burn scars. Note that the final burn scars mapped by this method are sensitive to the selection of the coefficient value. It was determined experimentally that the substantially low threshold compared to that used in active fire detection maintains a low level of commission error in the identification of BSPs. If the first test is false, and the pixel was a hotspot pixel on D1 and (T3–T4) ≤ 14 K, then the pixel also automatically becomes a confirmed BSP on D2. Confirmed BSPs and potential BSPs on D2 all pass to the final stage for confirmation.

*Confirmation (Fig. 1*d*)*

All non-wildland hotspots and burn scar pixels are masked out using a land cover type map (the Gap Analysis Project (GAP) vegetation dataset (Anderson *et al*. 1976; Holland 1986)). Open land, urban, agricultural cropland, dune and desert areas in California were here defined as non-wildland types while scrub, chaparral, grassland, marsh, riparian forest, woodland, rangeland and forests in California were defined as wildland classes in this analysis. Single hotspot and potential BSP pixels are then eliminated. It is assumed that in most situations single fire pixels and BSPs might be caused by subpixel fire contamination and/or other noise as well as by an image registration error between two consecutive days. For example, a forest pixel containing a fraction of water body along the edge of a lake may contain insufficient sun glint to be eliminated in earlier stages but will be removed at this stage. It is likely that those false single fires and BSPs distributing along boundaries of different land cover types are caused by possible subpixel registration errors. Therefore, it is reasonable to eliminate the single hotspot and/or BSP pixels at the final confirmation stage because the subpixel registration error between two consecutive days always exists in this dynamic algorithm. If the registration error of image to image is more than one pixel, this dynamic algorithm may cause a greater burn scar mapping error than other methods, such as MHANDS (a modified version of HANDS of Fraser *et al*. 2000) addressed as below. For this case, the algorithm may fail to produce a reliable result; users should be aware of this limitation.

An iterative procedure is used in BSP confirmation. A potential BSP is confirmed by a neighbour hotspot (within an 8-pixel neighbourhood) and in subsequent iterations by one to four previously confirmed neighbouring BSPs (including D1 hotspots and confirmed BSPs). In the first iteration a BSP can be confirmed by a neighbouring hotspot; in the second iteration it can be confirmed by either a neighbouring hotspot or a confirmed BSP; during the third to fifth iterations, it is confirmed by 2–4 confirmed BSPs; and after the fifth iteration, BSPs can be confirmed only by four confirmed neighbouring BSPs. After the confirmation stage, a real burn scar has to contain at least two hotspots (pixels). Finally, the cumulative hotspot map and burn scar map for D2 are stored and can be used as D1 data for the following day.

Results and analysis

The hotspot and burn scar results detected with daily AVHRR data for the two months in 1999 were produced simultaneously by the dynamic algorithm. For convenience, we analyse the hotspot and burn scar results separately.

Hotspot detection

To demonstrate the effectiveness of the dynamic algorithm, we compare the result from this algorithm with that generated by the MCCRS algorithm (Li *et al*. 2003) (originally developed by the Canadian Center for Remote Sensing (see Li *et al*. 2000*a*), but modified for use in California) (Fig. 2*b*). Because, compared to other existing algorithms, the CCRS algorithm produced superior results when employed to detect fires in the Canadian boreal forest (Li *et al*. 2000*a*), we modified the CCRS algorithm for wildfire detection in California. The MCCRS algorithm is also being considered for use in our North America historical forest fire mapping project (Li *et al*. 2003), sponsored by NASA (National Aeronautic and Space Administration), USA. Figure 2*a* presents an AVHRR composite image (R2/R2/R1 *v.* R/G/B) showing three active fires (three red circles) on 02 September 1999, in northern California, used as a locative reference and background for the results presented (hotspot composites and burn scar map) below. Figure 2*b*,*c* shows hotspot composites of the area over the two months, produced by the MCCRS and the dynamic algorithms respectively. The black lines in the figure represent fire polygon boundaries from CDF, and the light shadow areas both inside and outside the polygons are hotspots detected by the algorithms.

Compared to the satellite images and limited CDF fire polygons, the total hotspots detected by the two algorithms appear similar. The number of hotspots detected is 890 pixels for the MCCRS algorithm and 989 pixels for the dynamic algorithm. Most hotspots detected by the two algorithms are inside fire polygons, although some are outside. Despite the similarity of total detected hotspots, the hotspot distribution of the MCCRS is slightly different from that of the dynamic algorithm. It is evident that the hotspot distribution produced by the dynamic algorithm looks more reasonable than that of the MCCRS algorithm, especially in the burn scars labelled as A and C and for areas in southern California (the wildland fire detection results for southern California

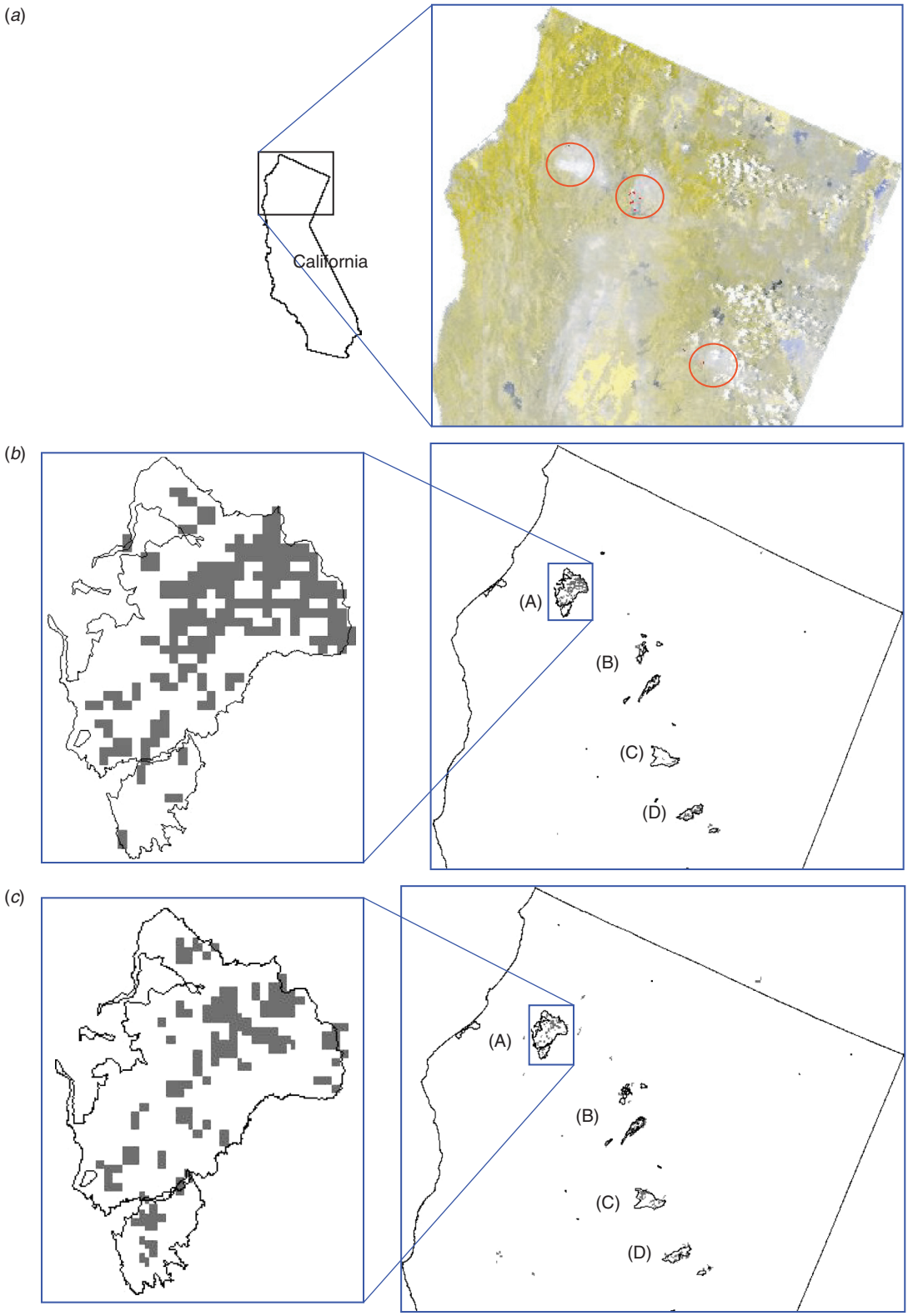

Fig. 2. AVHRR composite image (R2/R2/R1 *v.* R/G/B) showing three active fires in red circles on 02 September 1999, northern California, USA (*a*), and hotspot composite results for September and October of 1999, generated by the MCCRS algorithm (*b*) and the dynamic algorithm (*c*). The zoom-in fire polygon (A) in (*b*) and (*c*) burned around 50 days from 01 September to 20 October 1999. The black lines in the figure represent fire polygon boundaries from CDF and the light shadow areas both within and outside the polygons are hotspots detected by the algorithms.

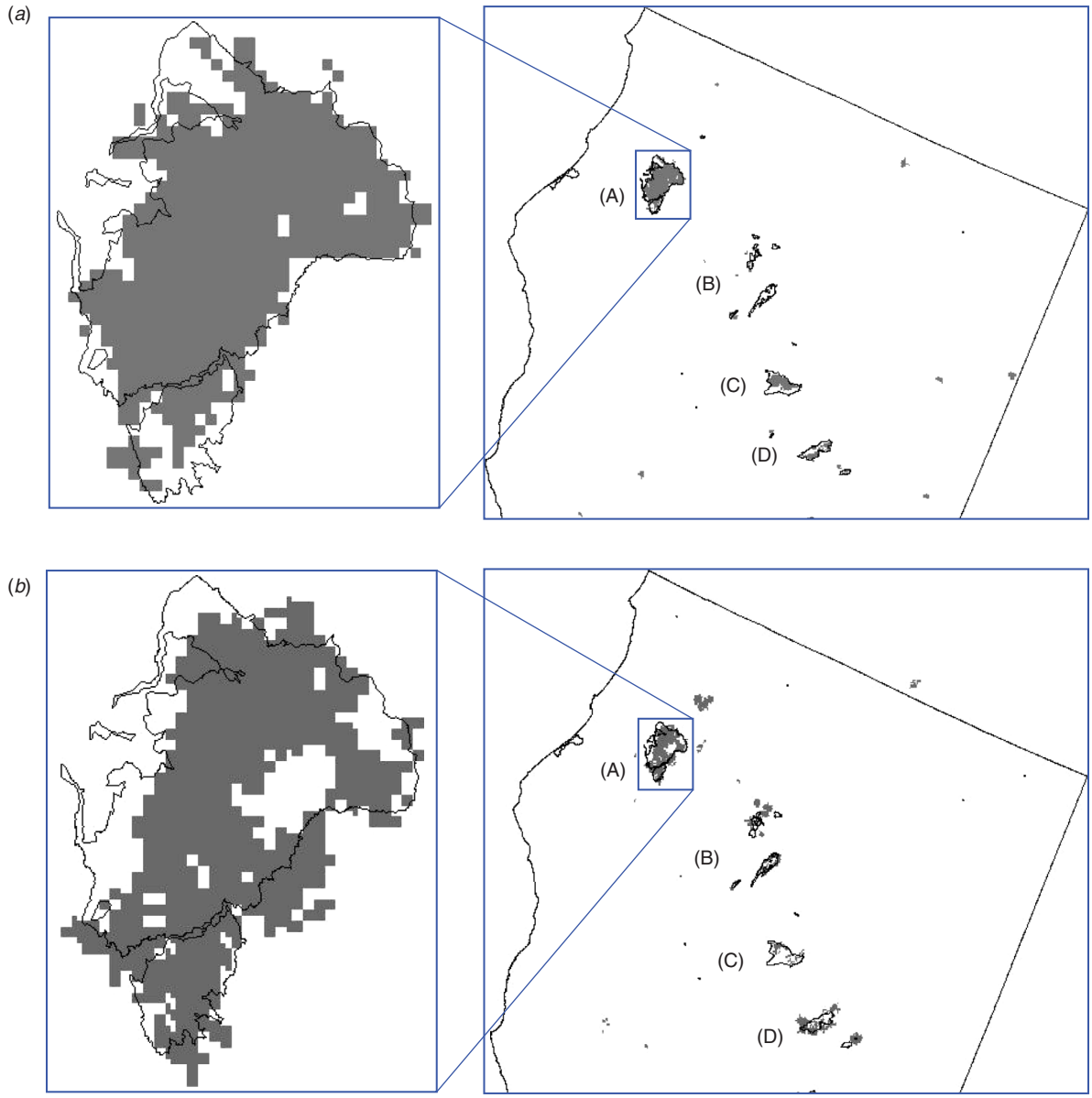

Fig. 3. Burn scar mapping results of September and October 1999 using the MHANDS algorithm (*a*) and the dynamic algorithm (*b*). The black lines in the figure represent fire polygon boundaries from CDF and the light shadow areas both within and outside the polygons are burn scars detected by the MHANDS and the dynamic algorithm.

are not shown in relevant figures in this paper). We compared the algorithms at the fire detection stage and found that the (NDVIdiff < (mean + 1.0 * s.d.)) condition in our dynamic algorithm could filter out many false alarms. We have demonstrated this point in the burn scar mapping with MHANDS, although we do not present the result in this paper.

Burn scar detection

Figure 3 shows a part of the burn scar mapping results generated by the MHANDS algorithm and the dynamic algorithm. With the dynamic algorithm, a total of 2281 km^2 of burn scars was mapped for the two months September and October 1999. Previous studies have shown that a pixel does behave spectrally as a 'burnt pixel' when at least 50% of the land surface covered by the pixel is burnt. Therefore, when considering the fact and comparing our mapping result (2281 km^2) to an incomplete dataset (incomplete coverage of the entire state of California) of ~1800 km^2 from the CDF fire polygons, we think that the mapped result seems reliable because we calculated burn scars at the pixel level. In addition, compared to the result (2227 km^2, Fig. 3*a*) generated by the MHANDS algorithm for the 2 months, the result produced by the dynamic algorithm looks reasonable (Fig. 3*b*). The major differences between MHANDS and HANDS are: separate

calculation of means and standard deviations of NDVI decrease for the different land cover types, and use of a different iteration algorithm for confirming a potential burn scar pixel. After conducting a closer examination of the distribution of burn scars mapped from Fig. 3 and a closer comparison between burn scars mapped by the dynamic method and CDF fire polygons, we can easily see that neither of the burn scar areas produced by the two methods (MHANDS and dynamic) fill the corresponding CDF fire polygons fully. Although the distributions of the burn scars mapped by the MHANDS method look better than those of the dynamic method for the burn scars labelled as A and C (Fig. 3*a* compared with 3*b*), the MHANDS method fails to map the burn scar labelled as B. Therefore, both algorithms had a similar capability for mapping the total burn scars in this experiment.

In Fig. 3*b*, the burn scar labelled as A matches well with its corresponding CDF fire polygon. Mapped burn scars B and D seem larger than the CDF fire polygons, while the area labelled C has less burnt acreage than the CDF fire polygon. To track the evolution of burned area mapped by the dynamic algorithm and to gain insight into the difference in burn scars mapped, we examined the time series of AVHRR composite images corresponding to the three fire events mapped by the dynamic algorithm (labelled as B, C and D in Fig. 3) that did not match the CDF fire polygons. For burn scar D, burning lasted ~20 days (almost all cloud-free), beginning on 28 August 1999. The hotspots detected in the period correspond to a larger burned area than the CDF fire polygon, mapped by the dynamic algorithm. For the burn scar labelled as B, the upper area burned from 02 to 20 September and smoke from this area appeared almost every day in the period, while the lower area burned for 5 days (16–20 October) with a couple of days having clouds over the area. Therefore, a burned area greater than the CDF fire polygons indicate seems reasonable, at least for the upper area in B (based on its daily visual smoke). For the burn scar C, it is apparent that the dynamic algorithm failed to map many burnt pixels. This is because there were three cloudy days during the 5-day burning (28 September–02 October), which led to missing the mapping of many burnt pixels. However, for the burn scar C in Fig. 3*a*, due to using NDVI composites before September and after October, the burn scar was mapped better with the MHANDS algorithm than with the dynamic algorithm (Fig. 3*b*).

Evolution of wildfires

A major advantage of using the dynamic algorithm is being able to monitor development of a wildfire event to a certain degree. Daily cumulative hotspot and burn scar results can be obtained (note that the daily cumulative hotspot result can also be obtained through single day hotspot detection, see Li *et al*. 2000*a*). Figure 4 illustrates the two curves of daily cumulative results detected during September and October 1999 in California. From the figure, it is easy to monitor the growing hotspot and burn scar trends over time. The results in Fig. 4 imply that the hotspots that the dynamic algorithm detects make up ~40–60% of the entire burn scars. The figure also provides some information about the severity of fire damage over time based on the slope information of the cumulative curves. For example, the burn scar curve from day 257 to day 272 grows faster than other days, especially during the period from day 270 to day 272.

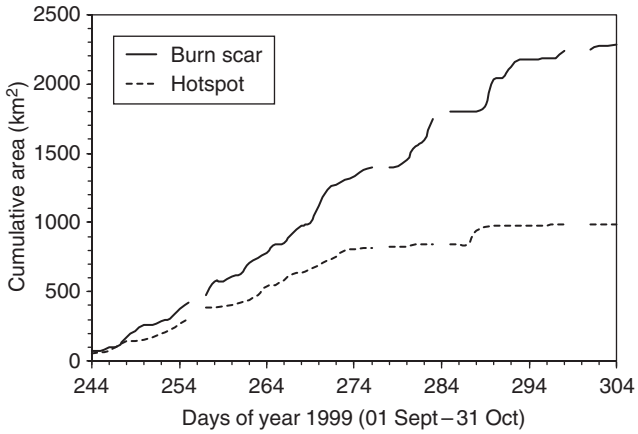

Fig. 4. Daily cumulative results of hotspot and burn scars from 01 September to 31 October 1999, generated by the dynamic algorithm.

Figure 5 shows both the spatial and the temporal evolution of hotspots and burn scars detected by the dynamic algorithm. Due to visual identification's limitation to colours, we show only the evolution of hotspots and burn scars in intervals spanning several days: 01–05 September in blue, 06–10 September in cyan, 11–15 September in green, 16–20 September in yellow, 21–30 September in brown, 01–10 October in pink, 11–20 October in red and 21–30 October in purple. From the zoom-in plots in the figure, it is immediately obvious that both hotspots and burn scars evolved in a north-west direction. The evolution information of wildfire, obtained through the dynamic algorithm, is useful for monitoring the spatial and temporal patterns of fire activity and development of a fire event throughout the study area and within a particular time interval. Consequently, these mapped results can finally help us monitor the development of hotspots and burn scars both in space and in time.

Validation issue

While many fire algorithms have been proposed, only a small number of them have been rigorously validated. In most cases, only cursory validations were conducted by comparing detected hotspots against fire smoke plumes (Li and Giglio 1999), due to the lack of ground truth in most regions. Therefore, validation of fire detection algorithms remains an outstanding issue. In this study, we used a dataset of CDF fire polygons to validate the mapping result by the dynamic algorithm. However, due to the fact that the CDF fire dataset

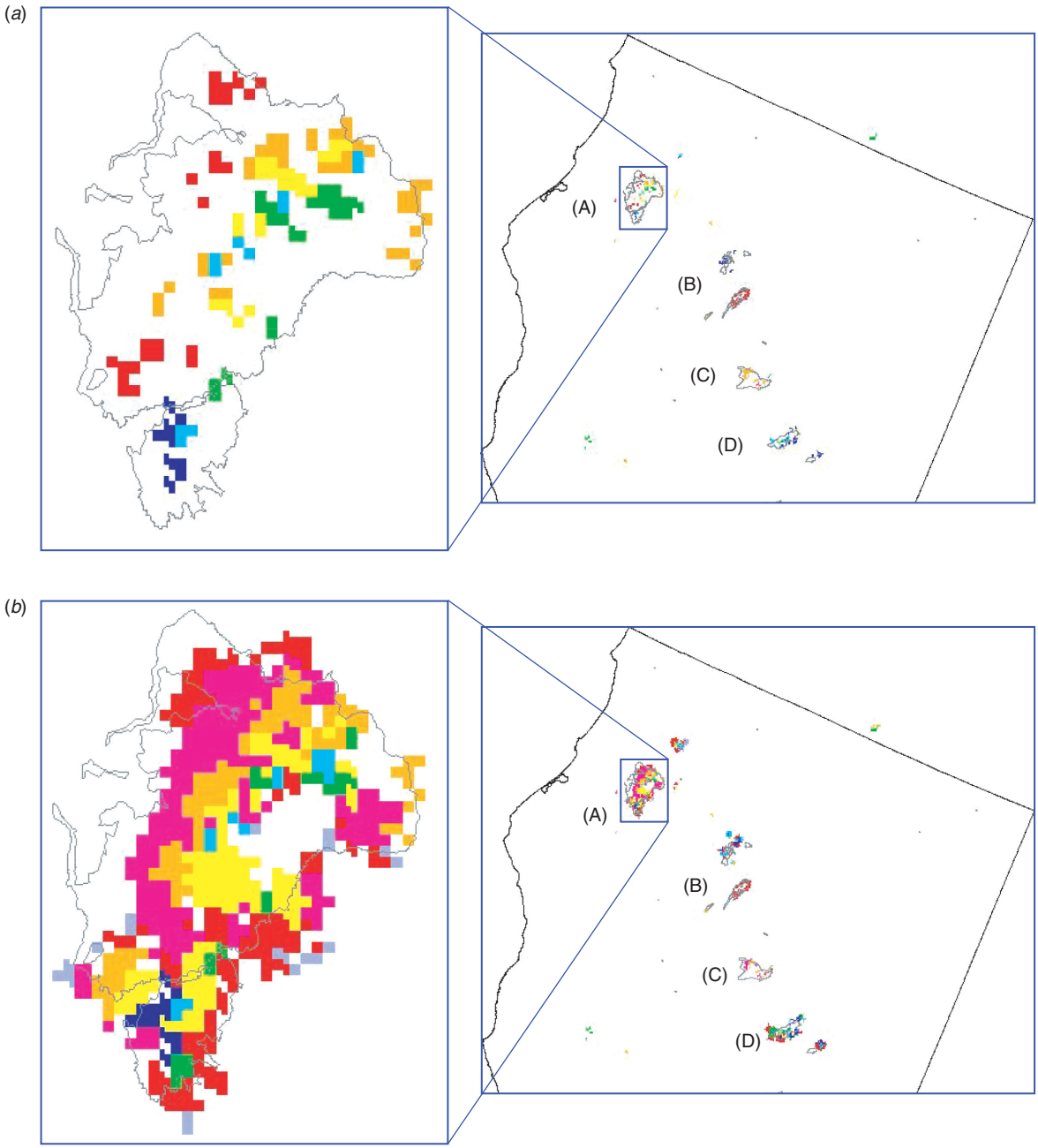

Fig. 5. Evolution maps of hotspots and burn scars in different colours: 01–05 September, blue; 06–10 September, cyan; 11–15 September, green; 16–20 September, yellow; 21–30 September, brown; 01–10 October, pink; 11–20 October, red; and 21–31 October, purple. (*a*) Hotspot evolution map. (*b*) Burn scar evolution map.

does not make a complete coverage of the entire state of California (missing data over some areas) and is inconsistent for its coordinates (with some degree of geo-location error) among all fire polygons, those fire polygon boundaries shown in Figs 2, 3 and 5 are just used as a general reference and cannot be used for any exact verification of the results mapped by the dynamic algorithm. In addition, the comparison of the results generated by the MHANDS and dynamic algorithms is also used as a general cross-validation between algorithms.

Conclusions

The preliminary comparisons between mapped results of the dynamic algorithm and CDF fire polygons and between the two wildfire mapping algorithms (MHANDS and dynamic), as well as visual examination of AVHRR

composite images, all indicate the potential of the dynamic algorithm to track burn scars at different stages of development and to produce a total burned area and hotspots similar to those produced by other algorithms. The dynamic algorithm appears to be able not only to produce daily cumulative hotspots but also to map daily cumulative burned area. The latter is the major contribution of this algorithm to wildfire detection methods. Therefore, the wildfire mapping result by the dynamic algorithm can be used to monitor evolution of wildfire activity both spatially and temporally. However, since the comparison of time series AVHRR data is sensitive to errors in multi-temporal image registration caused by the wide field of view of NOAA/AVHRR data (Roy 2000), etc., for the dynamic algorithm, a highly accurate registration system at the subpixel level is required.

Acknowledgements

This research is partially supported by California Air Resources Board, a NASA land cover and land use change grant, and an overseas distinguished Young Scientist Award of CAS, China.

References

Anderson JR, Hardy EE, Roach JT, Witmer RE (1976) 'A land use and land cover classification system for use with remote sensing data.' U.S. Geological Survey Professional Paper No. 964. (Washington, DC) 28 pp.

Andreae MO, Atlas E, Cachier H, Cofer WR III, Harris GW, Helas G, Koppmann R, Lacaux JP, Ward DE (1996) Trace gas and aerosol emissions from Savanna fires. In 'Biomass burning and global change, Vol. 1'. (Ed. JS Levine) pp. 278–295. (MIT Press: Cambridge, MA)

Arino O, Mellinotte JM (1998) The 1993 Africa fire map. *International Journal of Remote Sensing* **19**, 2019–2023. doi:10.1080/014311698214839

Arino O, Piccolini I, Siegert F, Eva H, Chuvieco E, Martin P, Li Z, Fraser RH, Kasischke E, Roy D, Pereira J, Stroppiana D (1999) Burn scars mapping methods. In 'Forest fire monitoring and mapping: a component of global observation of forest cover. Report of a workshop 3–5 November 1999'. (Eds F Ahern, J-M Grégoire, C Justice) pp. 198–223. (Joint Research Centre: Ispra, Italy)

Boles SH, Verbyla DL (2000) Comparison of three AVHRR-based fire detection algorithms for interior Alaska. *Remote Sensing of Environment* **72**, 1–16. doi:10.1016/S0034-4257(99)00079-6

Cahoon DR, Stocks BJ, Levine JS, Cofer WWR, Chung CC (1992) Evaluation of a technique for satellite-derived area estimation of forest fires. *Journal of Geophysical Research* **97**, 3805–3814.

Di L, Rundquist DC (1994) A one-step algorithm for correction and calibration of AVHRR level 1b data. *Photogrammetric Engineering and Remote Sensing* **60**, 165–171.

Dwyer E, Gregoire JM, Malingreau JP (1998) A global analysis of vegetation fires using satellite images: Spatial and temporal dynamics. *Ambio* **27**, 175–181.

Flannigan MD, Vonder Haar TH (1986) Forest fire monitoring using NOAA satellite AVHRR. *Canadian Journal of Forest Research* **16**, 975–982.

Flasse SP, Ceccato P (1996) A contextual algorithm for AVHRR fire detection. *International Journal of Remote Sensing* **17**, 419–424.

Franca JR, Brustet JM, Fontan J (1995) Multispectral remote sensing of biomass burning in West Africa. *Journal of Atmospheric Chemistry* **22**, 81–110.

Fraser RH, Li Z (2002) Estimating fire-related parameters in boreal forest using SPOT VEGETATION. *Remote Sensing of Environment* **82**, 95–110. doi:10.1016/S0034-4257(02)00027-5

Fraser RH, Li Z, Cihlar J (2000) Hotspot and NDVI differencing synergy (HANDS): a new technique for burned area mapping. *Remote Sensing of Environment* **74**, 362–376. doi:10.1016/S0034-4257(00)00078-X

Giglio L, Kendall JD, Justice CO (1999) Evaluation of global fire detection using simulated AVHRR infrared data. *International Journal of Remote Sensing* **20**, 1947–1985. doi:10.1080/014311699212290

Harris AJL (1996) Towards automated fire monitoring from space: semi-automated mapping of the January 1994 New South Wales wildfires. *International Journal of Wildland Fire* **6**, 107–116.

Holland RF (1986) 'Preliminary descriptions of the terrestrial natural communities of California.' (State of California, The Resources Agency, Nongame Heritage Program, Dept Fish. & Game: Sacramento) 156 pp.

Justice CO, Dowty P (Eds) (1994) IGBP-Dros. Inf. Serv. satellite fire detection algorithm workshop technical report. IGBP-Dros. Inf. Serv. Working Paper No. 9, February, 1993. (NASA/GSFC: Greenbelt, MD)

Justice CO, Kendall JD, Dowty PR, Scholes RJ (1996) Satellite remote sensing of fires during the SAFARI campaign using NOAA advanced very high resolution radiometer data. *Journal of Geophysical Research* **101**, 23 851–23 863. doi:10.1029/95JD00623

Kaufman YJ, Tucker CJ, Fung I (1990) Remote sensing of biomass burning in the tropics. *Journal of Geophysical Research* **95**, 9927–9939.

Kaufman YJ, Justice CO, Flynn LP, Kendall JD, Prins EM, Giglio L, Ward DE, Menzel WP, Setzer AW (1998) Potential global fire monitoring from EOS-MODros. Inf. Serv. *Journal of Geophysical Research—Atmospheres* **103**, 32 215–32 238. doi:10.1029/98JD01644

Kennedy PJ, Belward AS, Gregoire JM (1994) An improved approach to fire monitoring in West Africa using AVHRR data. *International Journal of Remote Sensing* **15**, 2235–2255.

Khazenie N, Richardson KA (1993) Detection of oil fire smoke over water in the Persian Gulf region. *Photogrammetric Engineering and Remote Sensing* **59**, 1271–1276.

Lee TM, Tag PM (1990) Improved detection of hotspots using the AVHRR 3.7 μm channel. *Bulletin of The American Metrological Society* **71**, 1722–1730. doi:10.1175/1520-0477(1990)071<1722:IDOHUT>2.0.CO;2

Levine JS (Ed.) (1991) 'Global biomass burning: atmospheric, climatic, and biospheric implications.' (MIT Press: Cambridge, MA) 569 pp.

Li Z, Giglio L (1999) A review of AVHRR-based fire detection algorithms. In 'Forest fire monitoring and mapping: a component of global observation of forest cover. Report of a workshop 3–5 November 1999'. (Eds F Ahern, J-M Grégoire, C Justice) pp. 175–197. (Joint Research Centre: Ispra, Italy)

Li Z, Cihlar J, Moreau L, Huang F, Lee B (1997) Monitoring fire activities in the boreal ecosystem. *Journal of Geophysical Research* **102** (D24), 29 611–29 624.

Li Z, Nadon S, Cihlar J (2000*a*) Satellite-based detection of Canadian boreal forest fires: Development and application of the algorithm. *International Journal of Remote Sensing* **21**, 3057–3069. doi:10.1080/01431160050144956

Li Z, Nadon S, Cihlar J, Stocks B (2000*b*) Satellite-based mapping of Canadian boreal forest fires: Evaluation and comparison of algorithms. *International Journal of Remote Sensing* **21**, 3071–3082. doi:10.1080/01431160050144965

Li Z, Fraser R, Jin J, Abuelgasim AA, Csiszar I, Gong P, Pu R, Hao W (2003) Evaluation of algorithms for fire detection and mapping across North America from satellite. *Journal of Geophysical Research* **108** (D2), 4076. doi:10.1029/2001JD001377

Malingreau JP, Justice CO (Eds) (1997) 'Definition and implementation of a global fire product derived from AVHRR data.' 3rd IGBP-Dros. Inf. Serv. Fire Working Group Meeting Report. IGBP-Dros. Inf. Serv. Working Paper 17, Toulouse, France, 13–15 November 1996.

Muirhead K, Cracknell A (1985) Straw burning over Great Britain detected by AVHRR. *International Journal of Remote Sensing* **6**, 827–833.

Pereira JMC (1999) A comparative evaluation of NOAA/AVHRR vegetation indexes for burned surface detection and mapping. *IEEE Transactions on Geoscience and Remote Sensing* **37**, 1217–1226. doi:10.1109/36.739156

Pozo D, Olmo EJ, Alados-Arboledas L (1997) Fire detection and growth monitoring using a multitemporal technique on AVHRR mid-infrared and thermal channels. *Remote Sensing of Environment* **60**, 111–120. doi:10.1016/S0034-4257(96)00117-4

Rauste Y, Herland E, Frelander H, Soini K, Kuoremaki T, Ruokari A (1997) Satellite-based forest fire detection for fire control in boreal forests. *International Journal of Remote Sensing* **18**, 2641–2656. doi:10.1080/014311697217512

Roy DP, Giglio L, Kendall JD, Justice CO (1999) Multi-temporal active-fire based burn scar detection algorithm. *International Journal of Remote Sensing* **20**, 1031–1038. doi:10.1080/014311699213073

Roy DP (2000) The impact of misregistration upon composited wide field of view satellite data and implications for change detection. *IEEE Transactions on Geoscience and Remote Sensing* **38**, 2017–2032. doi:10.1109/36.851783

Roy DP, Lewis PE, Justice CO (2002) Burned area mapping using multi-temporal moderate spatial resolution data—a bi-directional reflectance model-based expectation approach. *Remote Sensing of Environment* **83**, 263–286. doi:10.1016/S0034-4257(02)00077-9

Setzer AW, Pereira MC (1991) Amazonian biomass burnings in 1987 and an estimate of their tropospheric emission. *Ambio* **20**, 19–22.

Stroppiana D, Pinnock S, Gregoire JM (2000) The global fire product: daily fire occurrence from April 1992 to December 1993 derived from NOAA AVHRR data. *International Journal of Remote Sensing* **21**, 1279–1288. doi:10.1080/014311600210173